energies

MDPI

Article

Curled-Skewed Wakes behind Yawed Wind Turbines Subject to Veered Inflow

Mohammadreza Mohammadi [1,*], Majid Bastankhah [1,*], Paul Fleming [2], Matthew Churchfield [2], Ervin Bossanyi [3,4], Lars Landberg [4] and Renzo Ruisi [4]

[1] Department of Engineering, Durham University, Durham DH1 3LE, UK
[2] National Wind Technology Center, National Renewable Energy Laboratory, Golden, CO 80401, USA
[3] Faculty of Engineering, Bristol University, Bristol BS8 1TS, UK
[4] DNV, One Linear Park, Avon Street, Bristol BS2 0PS, UK
* Correspondence: mxm755@alumni.bham.ac.uk (M.M.); majid.bastankhah@durham.ac.uk (M.B.)

Abstract: This work presents a new engineering analytical model that predicts the effect of both the turbine yaw misalignment and the inflow wind veer on the wake flow distribution downwind of a wind turbine. To consider the veered inflow, two methods were examined. In the first method, the curled shape of the wake due to the yaw offset is initially modelled. The wake shape is then laterally skewed at each height due to the wind veer based on the assumption that the turbine wake is transported downstream by the incoming flow. The second method is a more realistic approach that accounts for the effect of wind veer on the wind velocity direction and the yaw angle seen by the wind turbine. This models the wake region in a local coordinate system defined based on the wind direction at each height. A coordinate transformation is then performed to represent the wake flow distribution in the global coordinate system attached to the ground. The results show that while the two methods provide similar outputs for small variations in the wind direction across the rotor, the difference becomes more evident with an increase in wind veer. High-fidelity simulations for a turbine subject to a neutral atmospheric boundary layer were employed to validate model predictions for different operating conditions.

Keywords: analytical wake model; wind veer; Coriolis force; wind turbine; wake steering; yaw angle

Citation: Mohammadi, M.; Bastankhah, M.; Fleming, P.; Churchfield, M.; Bossanyi, E.; Landberg, L.; Ruisi, R. Curled-Skewed Wakes behind Yawed Wind Turbines Subject to Veered Inflow. *Energies* **2022**, *15*, 9135. https://doi.org/10.3390/en15239135

Academic Editor: Davide Astolfi

Received: 4 October 2022
Accepted: 2 November 2022
Published: 2 December 2022

1. Introduction

Growing concerns about climate change and increasing energy demand have made many countries set ambitious targets to develop the renewable energy industry to reduce their carbon emissions [1]. These targets have motivated countries to develop their wind turbine industry, and the wind energy capacity has grown four times larger in the 2010s worldwide [2]. Decades of research in design and optimisation have taken horizontal-axis wind turbine rotor technology to a relatively mature stage to achieve efficiency values near the theoretical limit [3,4]. In recent years, attention has been redirected from the rotor technology to wind-farm performance strategies to maximize their efficiency. One of the major issues in wind farm control is the power loss in the wind turbines due to the wake of upstream turbines, which causes 10% to 20% of total power loss in large offshore wind farms [5]. Consequently, an accurate estimate of wake velocity deficit and the power losses due to wake effects is a crucial element in wind farm optimization. Wind turbine wake flows are known to be strongly affected by atmospheric operating conditions [6]. This is why the physics of the atmospheric flow and its interaction with wind farms was highlighted as one of the three grand challenges facing the wind energy industry [7].

One of the major tools to understand the interaction of wind turbines with the atmospheric boundary layer is the turbulent-resolving numerical simulation techniques. Nevertheless, these tools are expensive and time-consuming, so they are not generally very useful for the active control of wind farms, which requires fast and accurate tools that can

be implemented in the highly variable atmospheric conditions. Alternatively, analytical engineering models derived from flow-governing equations (i.e., the conservation of mass and momentum) have shown a great potential to characterise wind turbine wake flows for a wide range of operating conditions with low computational costs [6].

The pioneering analytical model proposed by Jensen [8], and further developed in [9], suggested that the velocity deficit in the wake of a wind turbine can be represented through a top-hat-shaped profile, which was used for decades. Nevertheless, the assumption was challenged by recent studies that showed that the top-hat shape is not a realistic representative in the far-wake region, where downstream turbines are usually installed [10,11]. Alternatively, Bastankhah and Porté-Agel [10] suggested a Gaussian profile to represent the velocity deficit in the wake of a wind turbine, and subsequent studies showed the applicability of the model in the far-wake region, e.g., [12,13]. In an effort to increase the model accuracy in the near-wake region, more recent works [11,14] suggested a super-Gaussian model, which turns into the Gaussian profile in the far-wake region but provides better results in the near-wake. Nevertheless, in most current wind farm sites, downstream turbines are placed in the far-wake region, so both Gaussian and super-Gaussian models produce fairly similar results, while the former has the advantage of simplicity.

One of the important atmospheric boundary layer flow phenomena that is often ignored in engineering wake models for simplicity is the effect of vertical change in wind direction, known as wind veer, which is mainly driven by the Coriolis force, as shown in the seminal work of Ekman [15]. The amount of wind veer is highly dependent on many factors, including earth roughness, atmospheric boundary layer stability, diurnal/nocturnal periods, and seasons [16]. Recent studies have shown that this phenomenon is very common in offshore wind sites, where measurements reported that some level of wind veer is present as much as 70% of the time in a year [17]. The wind veer effect changes aerodynamic load distributions along the wind turbine blade. More importantly, the wind turbine wake cross section is skewed in the presence of the wind veer [18]. This is important as it affects the overlapping area of the wake with downwind turbines and thereby their power production. Although it is not agreed that the wind veer can positively or negatively influence the power generation in a wind farm [19–21], it is known that the wind turbine wake is substantially affected by the wind veer. In particular, the veer effect has become increasingly relevant as the wind energy industry is growing and targeting larger sizes of rotors. A larger ratio of the turbine rotor diameter to the atmospheric boundary layer thickness leads to a greater vertical variation in the wind direction across the rotor due to the wind veer [22].

There has been a debate in the wind energy research community about how the Coriolis force and also the wind veer impact wake flows at a farm scale. Some of the high-fidelity numerical simulations (e.g., [23,24]) showed a clockwise deflection of the wind farm wake (viewed from above) in the Northern Hemisphere, while others (e.g., [25,26]) suggested an anticlockwise deflection. Van der Laan and Sørensen [27] showed that the apparent difference in the wake deflection is mainly due to the fact that the Coriolis force introduces two opposing effects on wake flow physics. On the one hand, the reduction in the streamwise velocity in the turbine wake changes the balance of the Coriolis force with other terms in the momentum equation and results in an anticlockwise wake deflection. On the other hand, the increased level of turbulence in the wake promotes the mixing of the low-velocity wake region with the high-velocity flow at the top, which in turn leads to a clockwise deflection due to the wind veer. Therefore, depending on which effect is more dominant, numerical simulations may suggest a clockwise or anticlockwise deflection of the wake. Nevertheless, the focus of these studies was mainly on the deflection of wind farm wakes at the hub height, and it is of great interest to study the impact of wind veer on the three-dimensional wake structure of a single wind turbine.

The skewed shape of the wake cross section due to the wind veer was modelled by Abkar et al. [28]. This was achieved by extending the Gaussian wake model [10] and proposing a skewed Gaussian profile (rather than axisymmetric profile). The model assumes that

lateral wake deflection is a function of the incoming lateral velocity at each height, and the wake advection in the streamwise direction depends on the incoming streamwise velocity. Although this is a relatively simplistic assumption, which neglects the complexities of the turbulent flow in the wake, the model shows a reasonable agreement with the large eddy simulation (LES) [28]. However, it is unknown how well this simplification works in different ranges of wind veer and also if the wind turbine is subjected to yaw misalignment implemented in wake steering techniques.

In recent years, wake steering techniques (i.e., intentional operation of yaw misalignment to deflect the wake away from downstream wind turbines) have become a common method in wind farm control [29–33]. This strategy improves wind farm operation as a whole, rather than controlling each wind turbine as an isolated unit [34]. Both experiments and numerical simulations [31,35–43], among others, showed that yawed turbine wakes have a curled (kidney) cross-sectional shape, which is formed as a result of a counter-rotating vortex pair shedding from yawed rotors. To develop an analytical model that predicts this curled shape, Bastankhah et al. [44] modelled the wake edge as a thin vortex sheet, and its deformation was mathematically found with time by solving the vortex transport equation. This time evolution is then mapped to a spatial one using a characteristic convective velocity. The predicted wake shape is finally incorporated into a modified Gaussian profile to predict the wake flow distribution. Nevertheless, this model (called the vortex-sheet curled model hereafter) only predicts the effect of yaw offset on the wake structure and does not account for the vertical wind veer. Very recently, LES results from Narasimhan et al. [45] for a yawed turbine subject to wind veer have showed that the wind veer introduces an asymmetry in the curled shape of the wake. They showed that the vorticity generated by the wind veer can be removed to obtain results in agreement with those reported by [44] in the absence of veer. This suggests that the effect of wind veer on the wake flow distribution can be separated from the one caused by the yaw offset.

This paper contributes to this area of research by providing a detailed analysis on two different methods that can be used to include wind veer effects in analytical wake models. Model predictions will be compared and validated against the LES data.

The paper is structured as follows. The modelling development is described in Section 2, where the vortex-sheet curled model [44] is used as the starting point and the vertical wind veer element is then added and modeled through two methods. Section 3 discusses the LES setup. Section 4 then presents the model outputs compared with the LES simulations, and finally, conclusions are made in Section 5.

2. Methodology

2.1. Model Development

As mentioned in the previous section, the vortex-sheet curled model [44] only considers the effect of yaw misalignment on the wake. The model suggests that the velocity deficit Δu at a certain streamwise distance x from the turbine can be calculated as:

$$\frac{\Delta u}{u_h} = C(x) \exp\left[-\frac{(y-y_c)^2 + (z-z_h)^2}{2\sigma^2}\right], \quad (1)$$

where u_h is the inflow velocity at the turbine hub height z_h, C is the maximum velocity deficit at each x, y is the lateral distance from the rotor centre, z is the height above the ground, y_c is the lateral wake centre location, and σ is the wake width. The basic assumption of the vortex-sheet curled wake model is similar to the Gaussian model [10]; that is the velocity deficit profiles in the wake of a wind turbine can be expressed as a Gaussian distribution as in Equation (1). Nevertheless, this equation has two significant differences from what was proposed in the original Gaussian model [10] for unyawed turbines. The first difference is in the σ parameter (the wake width), which, in the curled wake model, is calculated as:

$$\sigma = kx + 0.4\xi, \quad (2)$$

where k is the wake expansion rate, and ξ is the wake shape function. The first term in the above equation (i.e., kx) that is also present in the wake model for unyawed turbines [10] denotes the wake expansion due to turbulence and energy entrainment from the outer flow. The second term (i.e., 0.4ξ) describes the wake shape deformation due to the presence of the counter-rotating vortex pair in wakes of yawed turbines. The wake shape function ξ is found by solving the vortex transport equation for the wake edge, modelled as a two-dimensional vortex sheet. According to this model, the wake of a yawed turbine is characterised by a universal curled shape, which depends on only two dimensionless parameters: dimensionless time $\hat{t}$ and rotation rate χ. These parameters are further described in the next section (Section 2.2).

The other difference between the vortex-sheet curled wake model [44] and the original Gaussian wake model [10] is the fact that the location of the wake centre y_c is considered to be different from the rotor centre due to the lateral wake deflection. The value of y_c is further modified in the current study to incorporate the veer effect. This approach is based on assuming the wake is transported downstream by the incoming streamwise velocity and is also deflected laterally by the lateral inflow wind velocity, as suggested by [28]. Accordingly, an additional deflection term is added to the lateral wake centre location (y_c) to take the veer effect into account. This method is called Method I hereafter, and it is explained in more detail in Section 2.3. This simplistic approach assumes that the wind veer can be studied separately from the yaw offset. This is an inaccurate assumption, as the wind veer changes the effective yaw angle experienced by the turbine at each height. Therefore, a more physically realistic approach (called Method II hereafter) is to consider the effect of wind veer on the variation in the wind velocity direction and the yaw angle relative to the turbine. Consequently, in Method II, the effective yaw angle of the wind turbine varies with height. The modification of the vortex-sheet curled wake model in Method II to account for the veer effect is elaborated in Section 2.4. Finally, a comparison between the output of the two methods is made in Section 2.5 for different values of wind veer.

2.2. The Vortex-Sheet Curled Wake Model

As our modelling in this work is built on the vortex-sheet curled wake model [44], the key input parameters and equations of this model are summarised here for the sake of completeness. Additionally, a flowchart is provided in Section 2.4 that provides a visual summary of the below inputs and equations.

The model input parameters are the yaw angle β, the turbine thrust coefficient C_T, the rotor radius R, the hub-height inflow velocity u_h, the incoming streamwise velocity vertical profile $u_{in}(z)$, the friction velocity u_*, the streamwise and lateral distance from the turbine (x and y, respectively), the height above the ground z, the hub height z_h, the tip–speed ratio λ, and the wake expansion rate k. The model employs Equations (3)–(12) to estimate the wake width (Equation (2)) at each location, which is eventually used to determine the velocity deficit profile Δu in Equation (1).

A summary of the model steps are as follows. For more details, an interested reader is referred to the original work [44].

1. An approximation for the initial wake shape $\widetilde{\xi_0}$ is calculated based on the rotor radius R, and the ratio of the expanded stream-tube area to the projected frontal area of the rotor A_* is calculated as:

$$A_* = \frac{1 + \sqrt{1 - C_T cos^2(\beta)}}{2\sqrt{1 - C_T cos^2(\beta)}}, \tag{3}$$

and

$$\widetilde{\xi_0} \approx R\sqrt{A_*}. \tag{4}$$

2. The dimensionless time $\hat{t}$ is determined as:

$$\hat{t}(x,z) \approx -1.44 \frac{u_h}{u_*} \frac{R}{\widetilde{\xi_0}} C_T cos^2(\beta) sin(\beta)[1 - exp(-0.35 \frac{u_*}{u_{in}(z)} \frac{x}{R})]. \tag{5}$$

3. The normalised wake centre location $\hat{y}_c$ can be found as:

$$\hat{y}_c = \frac{(\pi-1)|\hat{t}|^3 + 2\sqrt{3}\pi^2\hat{t}^2 + 48(\pi-1)^2|\hat{t}|}{2\pi(\pi-1)\hat{t}^2 + 4\sqrt{3}\pi^2|\hat{t}| + 96(\pi-1)^2} sgn(\hat{t}) - \frac{2}{\pi}\frac{\hat{t}}{[(z+z_h)/\widetilde{\xi}_0]^2 - 1}, \quad (6)$$

and the lateral wake centre location can be derived as:

$$y_c \approx \hat{y}_c\widetilde{\xi}_0. \quad (7)$$

4. The polar angle θ at each location is defined as:

$$\theta = tan^{-1}\frac{z-z_h}{y-y_c}. \quad (8)$$

5. The initial wake shape $\xi_0(\theta)$ is determined as:

$$\xi_0(\theta) = R\sqrt{(A_*)}\frac{|cos(\beta)|}{\sqrt{1-sin^2(\beta)sin^2(\theta)}}. \quad (9)$$

6. The wake shape function can then be found as:

$$\xi(\theta, x) = \xi_0(\theta)\hat{\xi}(\theta, \hat{t}), \quad (10)$$

where $\hat{\xi}(\theta, \hat{t})$ can be estimated either analytically [44] or through the following empirical estimation:

$$\hat{\xi}(\theta, \hat{t}) = 1 - a[c_1(\hat{t})cos2\theta + (c_2(\hat{t})\chi sin2\theta + c_3(\hat{t})cos3\theta) + (c_4(\hat{t})\chi^2 cos2\theta + c_5(\hat{t})\chi sin3\theta + c_6(\hat{t})cos2\theta + c_7(\hat{t})cos4\theta)], \quad (11)$$

where a and $c_1, c_2, c_3, c_4, c_5, c_6, c_7$ are empirical coefficients and can be obtained through the equations provided in the Appendix A. Moreover, χ is the rotation rate and can be obtained as:

$$\chi = \frac{1}{\lambda sin(\beta)}. \quad (12)$$

7. The wake width can be obtained as stated in Equation (2).
8. The $\widetilde{\sigma}^2$, which is an approximation of σ^2, can be obtained as:

$$\widetilde{\sigma}^2(x) = (kx + 0.4\widetilde{\xi}_0)(kx + 0.4\widetilde{\xi}_0 cos\beta). \quad (13)$$

9. The maximum velocity deficit $C(x)$ can be calculated as:

$$C(x) = 1 - \sqrt{1 - \frac{R^2 C_T cos^3(\beta)}{2\widetilde{\sigma}^2(x)}}. \quad (14)$$

10. Finally, the wake velocity deficit can be determined based on Equation (1).

2.3. Curled-Skewed Wake Model—Method I

In the following, we discuss how the vortex-sheet curled model is modified in Method I to account for the veer effect. As mentioned earlier, this method is based on the assumption that the effect of veer on the wake can be separated from yaw misalignment. We assume that the yaw angle is constant and does not change across the rotor, and the lateral wake deflection due to the lateral velocity component $v_{in}(z)$ (shown in Figure 1 by blue arrows) of the incoming flow can be calculated as [28]:

$$\Delta y(z) \approx v_{in}(z)\Delta t = v_{in}(z)(x/u_{in}(z)) = x\tan(\alpha(z)), \quad (15)$$

where Δy is the wake deflection due to the veer effect, u_{in} is the streamwise component of the incoming velocity, and α is the wind veer angle at each height z. Figure 1 shows a schematic of the curled wake indicated by red color due to the yaw misalignment in comparison with the curled-skewed wake shown by blue as a result of the combined effect of yaw and veer. It is worth noting that, akin to prior works (e.g., [18,28,46]), for convenience, the current study defines the coordinate system with respect to the wind direction at the hub height. Therefore, the wind veer angle and v_{in} are assumed to be zero at the hub height, as shown in Figure 1.

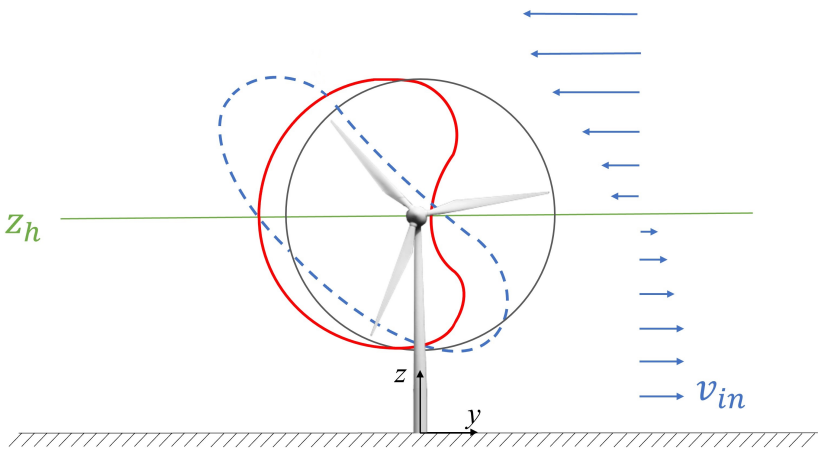

Figure 1. A schematic of the turbine and different wake shapes. The black circle shows the rotor disk, the red solid curve shows the curled wake shape due to yaw misalignment, the blue dashed curve shows the curled-skewed shape due to the combined effect of veer and yaw, and the blue arrows show the lateral wind velocity component, which varies with height.

If the veer term in Equation (15) is normalised by the initial wake size and is added to the wake centre location, the normalised lateral wake deflection due to veer can be obtained as $x\tan(\alpha(z))/\widetilde{\xi}_0$. Thus, if this term is added to Equation (6), the overall normalised wake defection, i.e., a combination of lateral deflection due to the yaw misalignment and due to wind veer, is given by:

$$\hat{y}(x,z) = \frac{(\pi-1)||\hat{t}|^3 + 2\sqrt{3}\pi^2\hat{t}^2 + 48(\pi-1)^2|\hat{t}|}{2\pi(\pi-1)\hat{t}^2 + 4\sqrt{3}\pi^2|\hat{t}| + 96(\pi-1)^2} sgn(\hat{t}) - \frac{2}{\pi}\frac{\hat{t}}{[(z+z_h)/\widetilde{\xi}_0(z)]^2 - 1} + \frac{xtan(\alpha(z))}{\widetilde{\xi}_0}. \quad (16)$$

If the above equation is inserted in the curled wake model and is used instead of Equation (6), the output can show the effect of yaw and veer together. A flowchart is provided in Section 2.4 to show these steps visually, together with other models/approaches discussed in this paper. While implementing the approach discussed above is rather straightforward, it is a remarkable simplification, as it overlooks the impact of the wind veer on the turbine yaw angle.

2.4. Curled-Skewed Wake Model—Method II

The second method is based on the fact that the yaw angle 'seen' by the turbine (hereafter, the effective yaw angle, γ) depends on the wind veer and therefore must change with height. The effective yaw angle γ at each height z is given by:

$$\gamma(z) = \beta + \alpha(z), \quad (17)$$

as shown in Figure 2. In the original vortex-sheet curled model [44], the streamwise direction is assumed to be parallel to the wind direction. In the case of wind veer, however,

the wind direction changes with the height. Therefore, in Method II, the curled model is written with respect to a local Cartesian coordinate system $(x_v - y_v)$, where the x_v-axis is in the direction of the incoming wind velocity at each height, and y_v is the horizontal direction normal to x_v, as shown in Figure 2. For each point in the absolute $(x - y)$ coordinate system (i.e., attached to the ground), where the x-axis is in the direction of the incoming wind velocity at the hub height, the corresponding values of x_v and y_v can be computed from:

$$x_v = xcos(\alpha(z)) + ysin(\alpha(z)), \tag{18}$$

$$y_v = -xsin(\alpha(z)) + ycos(\alpha(z)). \tag{19}$$

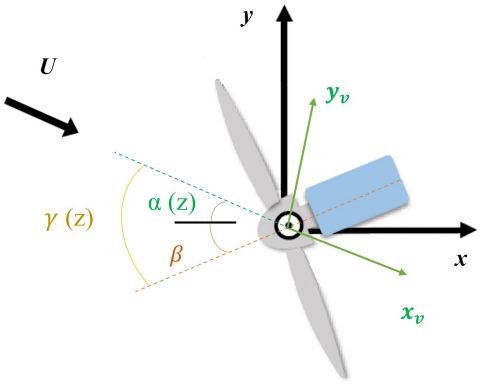

Figure 2. A schematic of the absolute coordinate system, which is independent of the veer angle $(x - y)$, and the local coordinate system, which is dependent on the veer angle $(x_v - y_v)$.

In Method II, similar Equations (1)–(14) are used to calculate the parameters for the vortex-sheet curled model at each height. There are, however, some notable differences with respect to the original vortex-sheet curled model. First, the effective yaw angle $\gamma(z)$ (defined in Equation (17)) is used instead of the yaw angle β in equations. Moreover, as discussed earlier, for each point in space, values of x_v and y_v are used in the vortex-sheet curled model instead of x and y. Finally, the u_h value in Equation (5) must be substituted by $u_{in}(z)$ since we use the curled model at each height with a different yaw angle. We would like to highlight a physical limitation of this approach. It essentially uses the vortex-sheet curled model on a horizontal plane at each height, whereas the original model was developed for the whole wake with its three-dimensional properties, including the wake rotation and the presence of a counter-rotating vortex pair. Due to the complexity of governing flow equations and the problem in hand, we were not able to mathematically solve equations and re-derive the vortex-sheet curled model for a vertically varying wind direction. Therefore, despite the fact that this assumption may introduce some uncertainty in model predictions, Method II seems to be a reasonable approach, and it enjoys a more robust physical basis compared to Method I.

Figure 3 provides a visual summary of the steps for all three versions of the vortex-sheet curled model, namely, the original yaw-only model [44] and the two yaw and veer models (Methods I and II) proposed in this work. As the figure shows, there are a number of turbine and inflow parameters that are required for all methods (the grey box). The input parameters, including the yaw angle β and the coordinate system x and y, are the same for both the original model (Section 2.2) and Method I (Section 2.3), while Method II (Section 2.4) uses the effective yaw angle γ as the input rather than β as well as local coordinate system x_v and y_v. Finally, as mentioned above, Method II uses $u_{in}(z)$ rather than u_h in Equation (5). In addition to the input parameters, there are a number of parameters that form the curled wake model platform and were introduced by [44] (the blue boxes). Accordingly, all three methods start with the calculation of A_* in Equation (3) and use the curled wake platform to end up with the velocity deficit values in Equation (1). The green

arrows should be followed for the original curled wake (i.e., yaw only) model, the orange arrows represent Method I, and the yellow arrows show Method II. Note the difference between Method I and the other two methods at this stage as the former uses a modified version of lateral wake centre deflection given in Equation (16) rather than the one based on Equation (6).

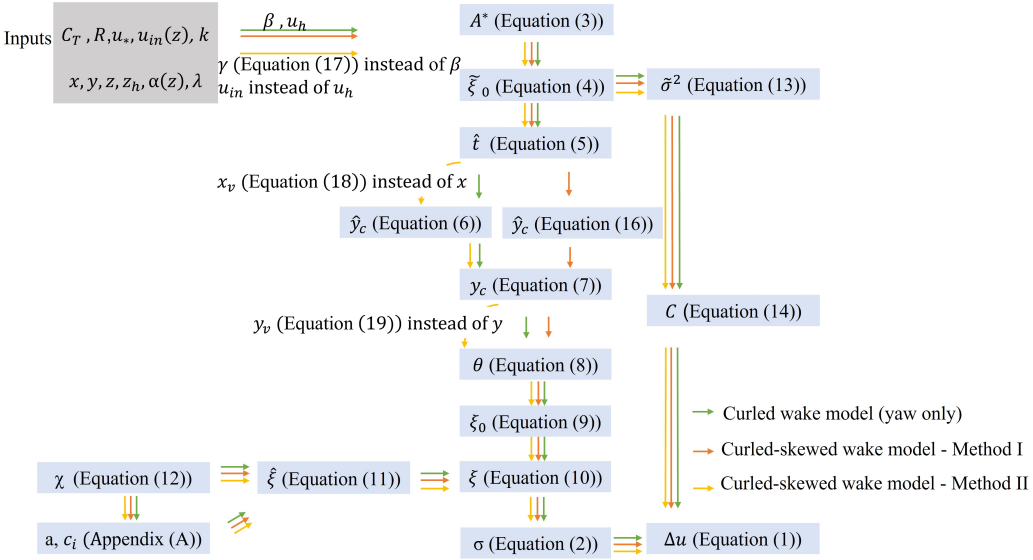

Figure 3. A flowchart showing the vortex-sheet curled wake model, curled-skewed wake model (Method I), and curled-skewed wake model (Method II).

2.5. Comparison between Method I and Method II

In this section, we compare predictions of the skewed-curled wake model based on both Methods I and II for a turbine with a thrust coefficient, C_T, of 0.66 and a yaw angle β of 25°. To make a fair comparison, the same inputs mentioned in Table 1 are used for both methods, where the wake recovery rate k is estimated by $0.6u_*/u_h$ [44].

Table 1. Input parameters for the analytical model.

Input Parameter	z_h(m)	u_h(m/s)	k	u_*(m/s)	λ
value	90	8.54	0.03	0.45	7.5

It is worth noting that the yaw angle is assumed to be positive if the rotor is misaligned in the anticlockwise direction, seen from above. Figure 4 shows contours of the wake velocity deficit Δu normalised by the incoming hub height velocity u_h at $x = 6D$. Results are shown in Figure 4 for a range of wind-direction variations across the rotor, selected based on atmospheric field measurements [17]. The value of $\bar{\alpha}$ is the variation in the wind direction across the rotor (i.e., from bottom tip to top tip), where $\bar{\alpha} = 0.05$, 0.1, 0.15, and 0.2 °/m. These are equivalent to 6.3, 12.6, 18.9, and 25.2 °/D, respectively, where $D = 126$ m for the National Renewable Energy Laboratory (NREL) 5-MW turbine [47] used in this study. The figure shows that for small and intermediate values of $\bar{\alpha} \leq 0.1$ °/m (i.e., $\bar{\alpha} \leq 12.6$ °/D), both methods predict relatively similar wake shapes, and their difference shown in the bottom subfigure is fairly small. However, more considerable differences can be observed for larger variations in the wind direction across the rotor, and their difference is no longer negligible for an inflow with strong veer of $\bar{\alpha} = 0.2$ °/m (i.e., $\bar{\alpha} = 25.2$ °/D).

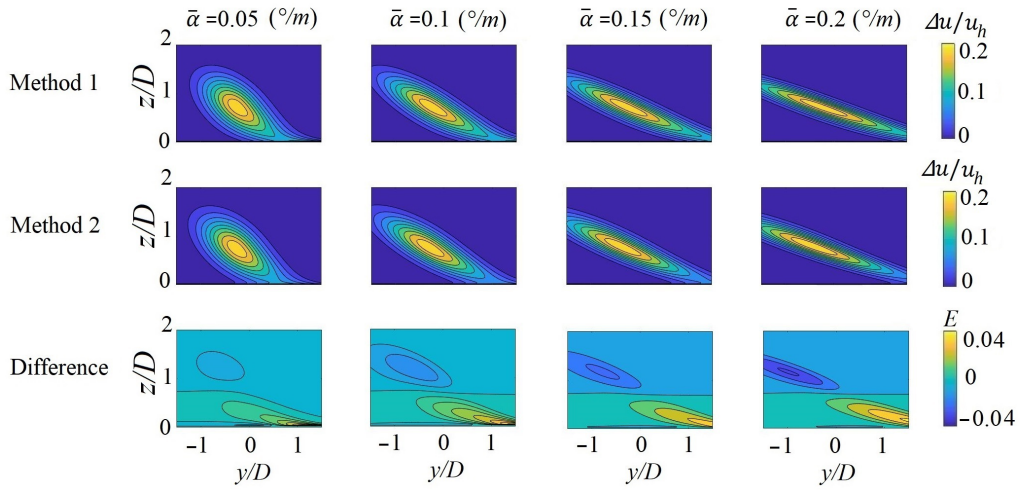

Figure 4. Contours of the normalised velocity deficit $\Delta u/u_h$ based on both Method I (top subfigure) and Method II (middle subfigure) at $x/D = 6$ for a turbine with a yaw angle of $\beta = 25^\circ$ and different veer angle variations $\bar{\alpha}$ across the rotor. The bottom subfigure shows the difference (E) in model predictions based on the two methods.

3. Large-Eddy Simulation Setup

We compared model predictions against the results of the LES performed with the Simulator for Wind Farm Applications (SOWFA) [48], which is a computational tool based on the Open FOAM CFD toolbox [49], together with the Fatigue, Aerodynamics, Structures, and Turbulence (FAST) turbine simulator tool [50]. Details about the simulation, techniques, and validation processes can be found in [29,51–53]. The simulated turbine was the NREL 5-MW turbine [47], where the hub height and the rotor diameter were 90 m and 126 m, respectively. Three different yaw angles, $\beta = 0^\circ$, 25°, and -25°, were modelled in this work, and the boundary layer was set in the neutral condition. The studied location was the Anholt wind farm site (56.5975° N, 11.1742° E), with the domain size of $x = 10{,}000$ m $\times$ $y = 5040$ m $\times$ $z = 2960$ m, where x, y, and z represent the streamwise, lateral, and vertical directions, respectively. In this location, the Coriolis parameter was $f_c = 1.20 \times 10^{-4}$ rad/s.

The inflow was provided through a precursor technique, where the simulation was first run without the turbine. These data were used in the turbine simulation as the inflow boundary conditions, while the downstream boundaries were considered as outflow [29]. The air density and aerodynamic surface roughness were set at 1.225 kg/m^3 and 0.03 m, respectively. In the LES data analysis, the streamwise velocity values on the vertical plane $(y - z)$ located at two rotor diameters upstream were used as the reference velocity for the velocity deficit contours, and the streamwise velocity of the incoming flow at the hub height was u_h = 8.54 m/s. It is worth noting that when the streamwise velocity values at two rotor diameters upstream were compared with the velocity values at the same y, z locations at three, four, five, and six rotor diameters upstream, the mean squared error was less than 0.002. Therefore, we use the inflow data at two rotor diameters to follow the industrial standard for velocity measurements at upstream locations [54].

Figure 5 shows inflow profiles of the time-averaged streamwise u and spanwise v velocity components, as well as the wind direction α. As seen in the figure, the wind veer changes from $\alpha = 3^\circ$ at the bottom tip to $\alpha = -2^\circ$ to the top tip, as a result of the Coriolis force ($\bar{\alpha} = 0.04\ ^\circ/\text{m} = 5\ ^\circ/D$). This amount of wind veer was chosen as the one that generates a 'typical' wind-direction variation across the rotor for a neutral atmospheric boundary layer; stronger than 'weak' wind veer angle variation ($\bar{\alpha} < 0.02\ ^\circ/\text{m}$) and smaller than 'substantial' variation ($\bar{\alpha} = 0.07 - 0.25\ ^\circ/\text{m}$) [17,18,22]. It is worth noting that a neutral atmospheric boundary layer is simulated in this work, but a more significant veer angle variation across the rotor is expected to be observed in a stable boundary layer as discussed in prior studies, e.g., [46]. For the veer range simulated in the LES, both Methods I and II

provide rather similar predictions, as shown in Figure 4. In the remainder of this study, we thus employ Method II due to its more robust underlying assumptions and compare its predictions with the LES results for the wake of yawed turbines subject to inflow veer.

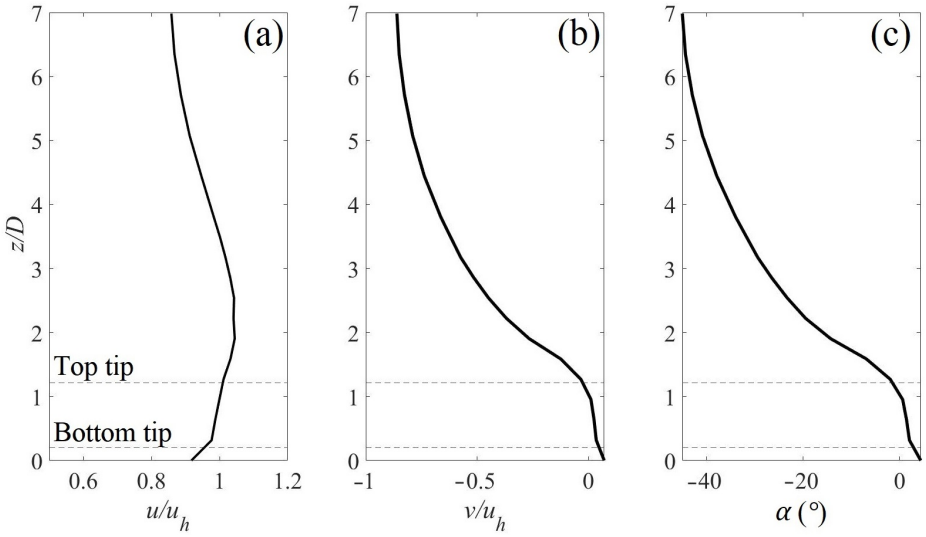

Figure 5. (**a**) The streamwise u and (**b**) the lateral v mean velocity components of the incoming velocities, normalised by u_h (**c**) Vertical profile of incoming wind direction α. The top tip and the bottom tip of the turbine are shown with dashed lines.

4. Results

Figures 6–8 show contours of the normalised velocity deficit $\Delta u/u_h$ in the wake of turbines with $\beta = 0°$, 25° and −25° for both the LES data and analytical model predictions. The turbine thrust coefficient for each case is computed from the LES data based on the definition given in [44]. This results in $C_T = 0.7$, 0.66, and 0.66 for cases with $\beta = 0°$, 25°, and −25°, respectively. Other input parameters of the analytical model are the same as those presented in Table 1.

The results show in all three cases that as the wake is advected downstream, it is deflected to the negative y values (i.e., clockwise deflection) above the hub height and to positive y values (i.e., anticlockwise deflection) below the hub height, causing a skewed shape due to the incoming wind veer. This is in agreement with the previous experimental and numerical studies on wake flows subjected to veered inflow [18,46,55,56]. In addition to the wake deformation caused by the wind veer, for yawed cases (Figures 7 and 8), a curled wake shape is formed because of the counter-rotating vortex pair behind the turbine [35,36]. Due to the lateral component of the thrust force in the case of yawed turbines (Figures 7 and 8), a noticeable lateral wake deflection at the hub height can be also observed, and the sign of this deflection expectedly depends on the direction of the yaw angle.

Comparing Figure 7 ($\beta = 25°$) with Figure 6 ($\beta = 0°$) shows that the combined effect of yaw and veer yields further lateral wake deflection above the hub height and reduced wake deflection below the hub height. On the other hand, in Figure 8 ($\beta = -25\,°$), the lateral deflection effect of yaw and veer are in the same direction below the hub height while at levels above the hub height their effects are in opposite directions. This finding is particularly important from an operation perspective, as in the veered inflow condition, the lateral deflection of the yawed turbine wake can be exaggerated or reduced depending on the yaw angle, the amount of veer, and the height from the ground.

It should be also noted that there is some discrepancy between the analytical model and the LES data, especially in the region near the turbine ($x/D = 4$), which has been also reported in previous works based on the Gaussian wake model [10]. This can be explained by the fact that velocity deficit profiles do not follow a Gaussian distribution in the wake

region near the turbine [41,57]. It can be seen that the model over-predicts the wake centre velocity deficit at $x/D = 4$.

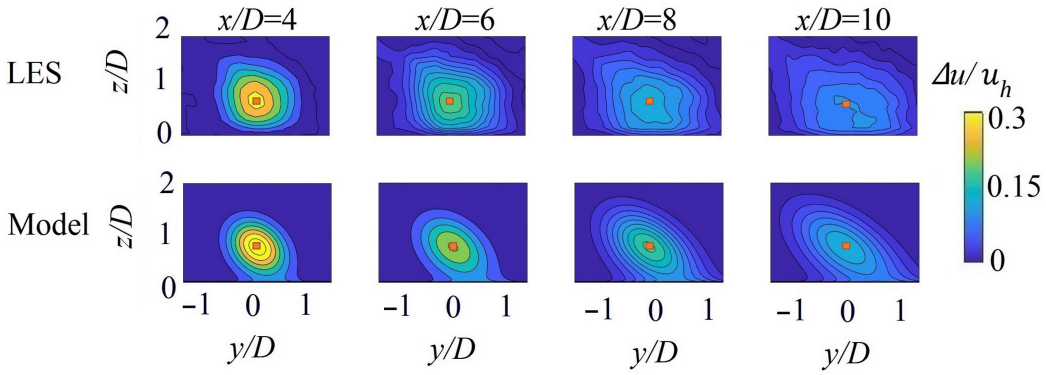

Figure 6. Contours of the normalised velocity deficit $\Delta u/u_h$ based on both LES (top subfigure) and the analytical model (bottom subfigure) at $x/D = 4$, 6, 8, and 10 for a turbine with a yaw angle of $\beta = 0°$ for $\bar{\alpha} = 0.04\,°/\mathrm{m}$, or, $5\,°/\mathrm{D}$. The square mark denotes the wake centre location.

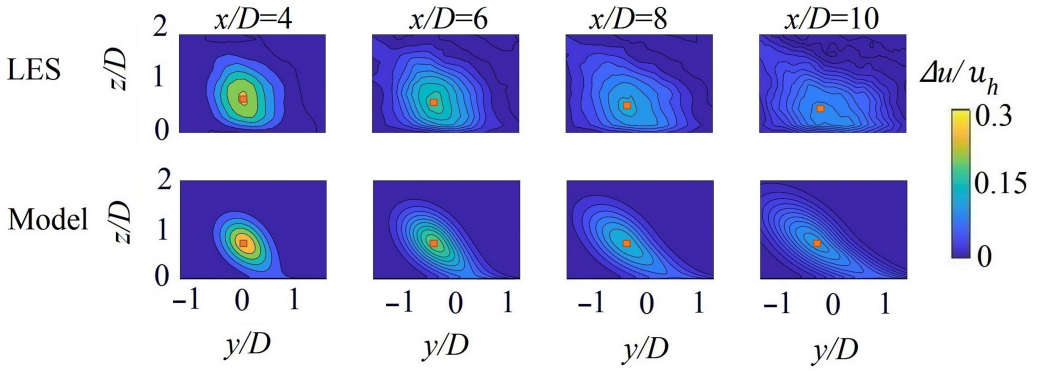

Figure 7. Contours of the normalised velocity deficit $\Delta u/u_h$ based on both LES (top subfigure) and the analytical model (bottom subfigure) at $x/D = 4$, 6, 8, and 10 for a turbine with a yaw angle of $\beta = 25°$ for $\bar{\alpha} = 0.04\,°/\mathrm{m}$, or, $5\,°/\mathrm{D}$. The square mark denotes the wake centre location.

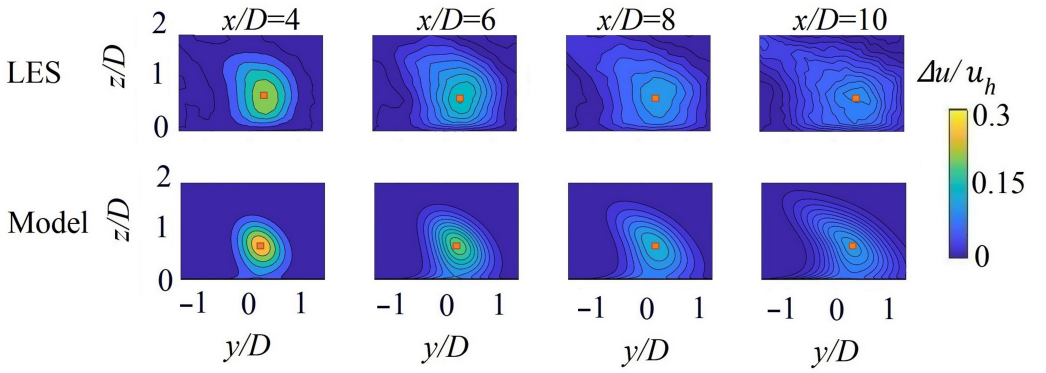

Figure 8. Contours of the normalised velocity deficit based on both LES (top subfigure) and the analytical model (bottom subfigure) at $x/D = 4$, 6, 8, and 10 for a turbine with a yaw angle of $\beta = -25°$ for $\bar{\alpha} = 0.04\,°/\mathrm{m}$, or, $5\,°/D$. The square mark denotes the wake centre location.

The analytical model and the LES results for the wake region are also used to evaluate the accuracy of the model to compute the available power for a downwind wind turbine. Figure 9a shows a schematic of a hypothetical turbine that is positioned behind the turbine for the three yawed cases ($\beta = 0°, 25°, -25°$) with $\bar{\alpha} = 0.04\,°/m$ (or, $5\,°/D$), simulated in

the LES. The streamwise wind velocity averaged over the frontal area of the hypothetical turbine is denoted by u_d and is used to estimate the available power ratio given by:

$$\frac{P}{P_0} = \left(\frac{u_d}{u_h}\right)^3, \tag{20}$$

where P is the available power for the hypothetical turbine, and P_0 is the available power for an unyawed turbine subject to the hub-height incoming velocity u_h. Figure 9b shows a comparison between the generated power of the hypothetical turbine predicted by the model versus the LES. As expected, the results show that the power generated by the hypothetical turbine is higher if the upwind turbine operates under yawed conditions given the lateral deflection of the wake. In addition to the normalised power, there is also a good agreement for the wake-centre velocity deficit C (calculated from Equation (14)) between the LES and the analytical model.

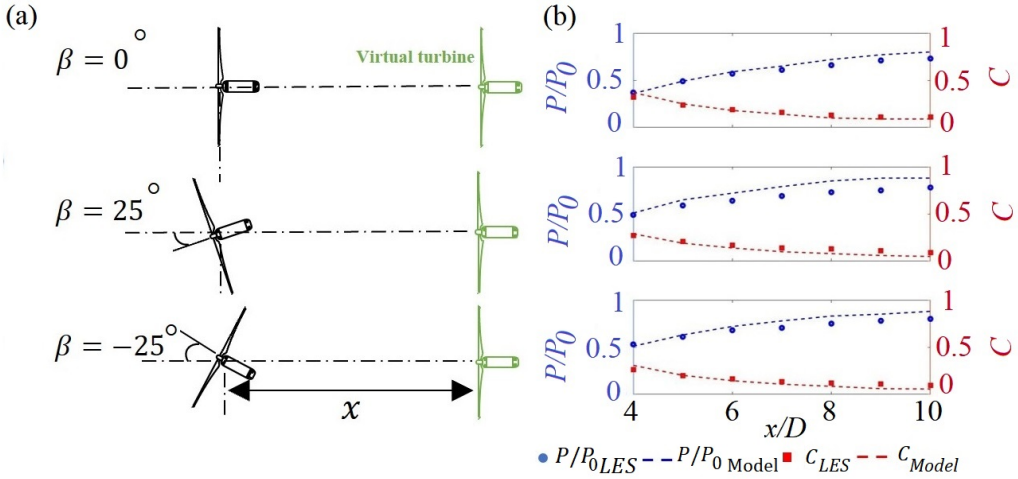

Figure 9. (**a**) A schematic of a virtual turbine placed downstream of a turbine in different yaw angles. (**b**) The normalised power generation by the virtual turbine together with the maximum velocity deficit at different streamwise distances from the turbine.

The focus of this paper is to investigate how the wind veer deforms the curled shape of a yawed wind turbine wake. The other potential effect of the wind veer however can be the lateral deflection of the wake centre at the hub-height level due to the turbulent mixing with the flow at the top of the turbine, as shown in previous wind farm studies, e.g., [27] and discussed in the introduction. It is of interest to use our LES data to examine whether the veer can introduce any noticeable wake deflection at the hub height for a single turbine. Figure 10 shows contours of the normalised streamwise velocity u/u_h on a horizontal plane at the hub height behind a single unyawed turbine for three different veer conditions; $\bar{\alpha} = 0\ ^\circ$/m, $\bar{\alpha} = 0.02\ ^\circ$/m, or, 2.5 $^\circ$/D, and $\bar{\alpha} = 0.04\ ^\circ$/m, or, 5 $^\circ$/D. The trajectory of the wake centre is also shown with a dashed line in the figure. One can observe that the presence of the wind veer does not lead to any noteworthy lateral deflection at the hub height level for small and intermediate values of wind-direction variation across the rotor. Therefore, our LES data suggest that the wind veer is mainly responsible for the deformation of the wake cross section, causing a skewed wake shape, for a single wind turbine rather than deflecting it at the hub-height in a horizontal plane. It is, however, essential to perform LES in future studies for a range of stable boundary layers with stronger variations in wind direction across the rotor to have a more comprehensive conclusion.

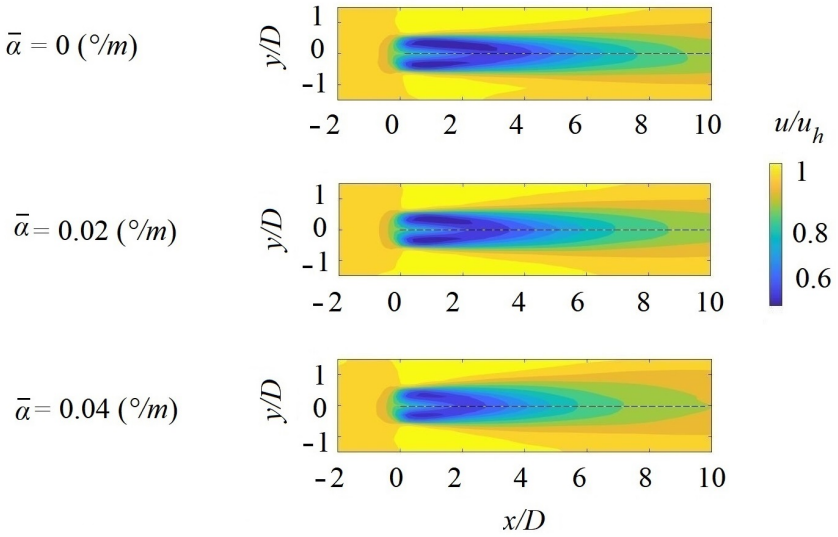

Figure 10. Contours of the normalised streamwise velocity u/u_h downwind of an unyawed turbine on a horizontal plane at the hub height for $\bar{\alpha} = 0\,^\circ/\mathrm{m}$, $\bar{\alpha} = 0.02\,^\circ/\mathrm{m}$, and $\bar{\alpha} = 0.04\,^\circ/\mathrm{m}$. The dashed lines indicate the wake centre trajectory.

5. Summary

In this paper, a fast-running engineering model is developed to describe how the wake structure is affected by both the inflow wind veer and the turbine yaw misalignment. Intentional operation of wind turbines under yawed conditions has recently become a common wake-mitigation strategy. The wind veer is also an important feature of the atmospheric boundary layer [17,58]. The developed model is thus expected to be useful for wind farm optimisation purposes, as it provides a more realistic estimation of the wake velocity deficit. The current work is built on the recently developed vortex-sheet model [44] that predicts the curled shape of the wake under yawed conditions. Two methods are studied to extend this analytical model and include wind veer effects on turbine wakes. Method I assumes that the effect of wind veer and yaw offset on the turbine wake can be modelled separately. In Method II, we take into account the fact that the wind veer changes the effective yaw angle seen by the turbine at each height. Model predictions are first obtained on a local coordinate system aligned with the wind direction at each height. The three-dimensional wake flow field is then reconstructed by applying a coordinate transformation. The results showed that there is a large difference in outputs (≈20%) of the two methods for cases with strong wind veer. However, at low and medium wind direction variations across the rotor ($\bar{\alpha} < 0.1\,^\circ/\mathrm{m}$, or, $12.6\,^\circ/\mathrm{D}$), the discrepancy is less significant (<5%). This work suggests that Method II is a more physically realistic method, and it is recommended for wind farm control applications. Model outputs are validated against the LES results for a turbine immersed in a neutral atmospheric boundary layer with three different yaw angles. It is also shown that the model is able to accurately predict the available power for a hypothetical turbine located at various downwind positions.

Author Contributions: Conceptualization, M.B., M.M., E.B., L.L. and R.R.; methodology, M.M. and M.B.; LES software, P.F. and M.C.; LES validation, P.F. and M.C.; formal analysis, M.M.; investigation, M.M. and M.B.; resources, M.M., M.B., P.F., M.C., E.B., L.L. and R.R.; data curation, M.M.; writing—original draft preparation, M.M.; writing—review and editing, M.M., M.B. and E.B., supervision, M.B., R.R. and E.B.; project administration, M.M., M.B., E.B. and L.L.; funding acquisition, M.B., E.B. and R.R. All authors have read and agreed to the published version of the manuscript.

Funding: This research was funded by Innovate UK no. 89640 (TS/V020773/1).

Institutional Review Board Statement: Not applicable.

Informed Consent Statement: Not applicable.

Data Availability Statement: Not applicable.

Acknowledgments: We acknowledge the funding received from Innovate UK (no. 89640) for the project entitled "CONtrol of FLOating wind farms with Wake Steering—CONFLOWS"; a collaboration between UK and US institutes to investigate wake steering for offshore wind turbines. This work was authored in part by the National Renewable Energy Laboratory, operated by Alliance for Sustainable Energy, LLC, for the U.S. Department of Energy (DOE) under Contract No. DE-AC36-08GO28308. Funding is provided by the U.S. Department of Energy Office of Energy Efficiency and Renewable Energy Wind Energy Technologies Office. The views expressed in the article do not necessarily represent the views of the DOE or the U.S. Government. The U.S. Government retains and the publisher, by accepting the article for publication, acknowledges that the U.S. Government retains a nonexclusive, paid-up, irrevocable, worldwide license to publish or reproduce the published form of this work or allow others to do so, for the U.S. Government purposes.

Conflicts of Interest: The authors declare no conflict of interest.

Appendix A

This appendix contains the empirical coefficients for Equation (11). The interested reader is referred to [44] for further information.

$$c_i(\hat{t}) = a_i tanh\frac{\hat{t}^{n_i}}{b_i} \tag{A1}$$

$$a = 1.263cos(0.33\chi) \tag{A2}$$

Table A1. Coefficients of the Equation (A1).

Term	1	2	3	4	5	6	7
a_i	1/2	−1/3	−1/4	−1/6	5/16	−5/48	7/48
b_i	4a	8a	8a	16a	16a	16a	16a
n_i	2	3	3	4	4	4	4

References

1. Obobisa, E.S. Achieving 1.5° C and net-zero emissions target: The role of renewable energy and financial development. *Renew. Energy* **2022**, *188*, 967–985. [CrossRef]
2. Roga, S.; Bardhan, S.; Kumar, Y.; Dubey, S.K. Recent technology and challenges of wind energy generation: A review. *Sustain. Energy Technol. Assess.* **2022**, *52*, 102239. [CrossRef]
3. Stevens, R.J.; Meneveau, C. Flow structure and turbulence in wind farms. *Annu. Rev. Fluid Mech.* **2017**, *49*, 311–339. [CrossRef]
4. Sørensen, J.N. The general momentum theory. In *General Momentum Theory for Horizontal Axis Wind Turbines*; Springer: Berlin/Heidelberg, Germany, 2016; pp. 43–58.
5. Barthelmie, R.J.; Hansen, K.; Frandsen, S.T.; Rathmann, O.; Schepers, J.; Schlez, W.; Phillips, J.; Rados, K.; Zervos, A.; Politis, E.; et al. Modelling and measuring flow and wind turbine wakes in large wind farms offshore. *Wind. Energy Int. J. Prog. Appl. Wind. Power Convers. Technol.* **2009**, *12*, 431–444. [CrossRef]
6. Porté-Agel, F.; Bastankhah, M.; Shamsoddin, S. Wind-turbine and wind-farm flows: A review. *Bound. Layer Meteorol.* **2020**, *174*, 1–59. [CrossRef] [PubMed]
7. Veers, P.; Dykes, K.; Lantz, E.; Barth, S.; Bottasso, C.L.; Carlson, O.; Clifton, A.; Green, J.; Green, P.; Holttinen, H.; et al. Grand challenges in the science of wind energy. *Science* **2019**, *366*, eaau2027. [CrossRef]
8. Jensen, N. *A Note on Wind Turbine Interaction*; Riso-M-2411; Risoe National Laboratory: Roskilde, Denmark, 1983; p. 16.
9. Katic, I.; Højstrup, J.; Jensen, N.O. A simple model for cluster efficiency. In Proceedings of the European Wind Energy Association Conference and Exhibition, Rome, Italy, 7–9 October ; Volume 1, pp. 407–410.
10. Bastankhah, M.; Porté-Agel, F. A new analytical model for wind-turbine wakes. *Renew. Energy* **2014**, *70*, 116–123. [CrossRef]
11. Schreiber, J.; Balbaa, A.; Bottasso, C.L. Brief communication: A double-Gaussian wake model. *Wind. Energy Sci.* **2020**, *5*, 237–244. [CrossRef]
12. Carbajo Fuertes, F.; Markfort, C.D.; Porté-Agel, F. Wind turbine wake characterization with nacelle-mounted wind lidars for analytical wake model validation. *Remote. Sens.* **2018**, *10*, 668. [CrossRef]
13. Teng, J.; Markfort, C.D. A calibration procedure for an analytical wake model using wind farm operational data. *Energies* **2020**, *13*, 3537. [CrossRef]

14. Shapiro, C.R.; Starke, G.M.; Meneveau, C.; Gayme, D.F. A wake modeling paradigm for wind farm design and control. *Energies* **2019**, *12*, 2956. [CrossRef]
15. Ekman, V.W. *On the Influence of the Earth's Rotation on Ocean-Currents*; Almqvist & Wiksells boktryckeri: Uppsala, Sweden, 1905 .
16. Brown, A.; Beljaars, A.; Hersbach, H.; Hollingsworth, A.; Miller, M.; Vasiljevic, D. Wind turning across the marine atmospheric boundary layer. *Q. J. R. Meteorol. Soc. J. Atmos. Sci. Appl. Meteorol. Phys. Oceanogr.* **2005**, *131*, 1233–1250. [CrossRef]
17. Bodini, N.; Lundquist, J.K.; Kirincich, A. US East Coast lidar measurements show offshore wind turbines will encounter very low atmospheric turbulence. *Geophys. Res. Lett.* **2019**, *46*, 5582–5591. [CrossRef]
18. Abkar, M.; Sharifi, A.; Porté-Agel, F. Wake flow in a wind farm during a diurnal cycle. *J. Turbul.* **2016**, *17*, 420–441. [CrossRef]
19. Choukulkar, A.; Pichugina, Y.; Clack, C.T.; Calhoun, R.; Banta, R.; Brewer, A.; Hardesty, M. A new formulation for rotor equivalent wind speed for wind resource assessment and wind power forecasting. *Wind. Energy* **2016**, *19*, 1439–1452. [CrossRef]
20. Bardal, L.M.; Sætran, L.R.; Wangsness, E. Performance test of a 3MW wind turbine–effects of shear and turbulence. *Energy Procedia* **2015**, *80*, 83–91. [CrossRef]
21. Eriksson, O.; Breton, S.P.; Nilsson, K.; Ivanell, S. Impact of wind veer and the Coriolis force for an idealized farm to farm interaction case. *Appl. Sci.* **2019**, *9*, 922. [CrossRef]
22. Gao, L.; Li, B.; Hong, J. Effect of wind veer on wind turbine power generation. *Phys. Fluids* **2021**, *33*, 015101. [CrossRef]
23. Lu, H.; Porté-Agel, F. Large-eddy simulation of a very large wind farm in a stable atmospheric boundary layer. *Phys. Fluids* **2011**, *23*, 065101. [CrossRef]
24. Churchfield, M.; Wang, Q.; Scholbrock, A.; Herges, T.; Mikkelsen, T.; Sjöholm, M. Using high-fidelity computational fluid dynamics to help design a wind turbine wake measurement experiment. *J. Phys. Conf. Ser.* **2016**, *753*, 032009. [CrossRef]
25. Dörenkämper, M.; Witha, B.; Steinfeld, G.; Heinemann, D.; Kühn, M. The impact of stable atmospheric boundary layers on wind-turbine wakes within offshore wind farms. *J. Wind. Eng. Ind. Aerodyn.* **2015**, *144*, 146–153. [CrossRef]
26. Allaerts, D.; Meyers, J. Boundary-layer development and gravity waves in conventionally neutral wind farms. *J. Fluid Mech.* **2017**, *814*, 95–130. [CrossRef]
27. van der Laan, M.P.; Sørensen, N.N. Why the Coriolis force turns a wind farm wake clockwise in the Northern Hemisphere. *Wind. Energy Sci.* **2017**, *2*, 285–294. [CrossRef]
28. Abkar, M.; Sørensen, J.N.; Porté-Agel, F. An analytical model for the effect of vertical wind veer on wind turbine wakes. *Energies* **2018**, *11*, 1838. [CrossRef]
29. Fleming, P.A.; Gebraad, P.M.; Lee, S.; van Wingerden, J.W.; Johnson, K.; Churchfield, M.; Michalakes, J.; Spalart, P.; Moriarty, P. Evaluating techniques for redirecting turbine wakes using SOWFA. *Renew. Energy* **2014**, *70*, 211–218. [CrossRef]
30. Gebraad, P.M.; Teeuwisse, F.; Van Wingerden, J.; Fleming, P.A.; Ruben, S.; Marden, J.; Pao, L. Wind plant power optimization through yaw control using a parametric model for wake effects—A CFD simulation study. *Wind. Energy* **2016**, *19*, 95–114. [CrossRef]
31. Schottler, J.; Mühle, F.; Bartl, J.; Peinke, J.; Adaramola, M.S.; Sætran, L.; Hölling, M. Comparative study on the wake deflection behind yawed wind turbine models. *J. Phys. Conf. Ser.* **2017**, *854*, 012032. [CrossRef]
32. Fleming, P.; King, J.; Dykes, K.; Simley, E.; Roadman, J.; Scholbrock, A.; Murphy, P.; Lundquist, J.K.; Moriarty, P.; Fleming, K.; et al. Initial results from a field campaign of wake steering applied at a commercial wind farm–Part 1. Wind Energy Science **2019**, *4*, 273–285. [CrossRef]
33. Campagnolo, F.; Petrović, V.; Schreiber, J.; Nanos, E.M.; Croce, A.; Bottasso, C.L. Wind tunnel testing of a closed-loop wake deflection controller for wind farm power maximization. *J. Phys. Conf. Ser.* **2016**, *753*, 032006. [CrossRef]
34. Bastankhah, M.; Porté-Agel, F. Wind farm power optimization via yaw angle control: A wind tunnel study. *J. Renew. Sustain. Energy* **2019**, *11*, 023301. [CrossRef]
35. Howland, M.F.; Bossuyt, J.; Martínez-Tossas, L.A.; Meyers, J.; Meneveau, C. Wake structure in actuator disk models of wind turbines in yaw under uniform inflow conditions. *J. Renew. Sustain. Energy* **2016**, *8*, 043301. [CrossRef]
36. Bastankhah, M.; Porté-Agel, F. Experimental and theoretical study of wind turbine wakes in yawed conditions. *J. Fluid Mech.* **2016**, *806*, 506–541. [CrossRef]
37. Bartl, J.; Mühle, F.; Schottler, J.; Sætran, L.; Peinke, J.; Adaramola, M.; Hölling, M. Wind tunnel experiments on wind turbine wakes in yaw: effects of inflow turbulence and shear. *Wind. Energy Sci.* **2018**, *3*, 329–343. [CrossRef]
38. Martínez-Tossas, L.A.; Annoni, J.; Fleming, P.A.; Churchfield, M.J. The aerodynamics of the curled wake: A simplified model in view of flow control. *Wind. Energy Sci.* **2019**, *4*, 127–138. [CrossRef]
39. Bossuyt, J.; Scott, R.; Ali, N.; Cal, R.B. Quantification of wake shape modulation and deflection for tilt and yaw misaligned wind turbines. *J. Fluid Mech.* **2021**, *917*, *A3* . [CrossRef]
40. Lin, M.; Porté-Agel, F. Large-eddy simulation of yawed wind-turbine wakes: comparisons with wind tunnel measurements and analytical wake models. *Energies* **2019**, *12*, 4574. [CrossRef]
41. Shapiro, C.R.; Gayme, D.F.; Meneveau, C. Modelling yawed wind turbine wakes: A lifting line approach. *J. Fluid Mech.* **2018**, *841*, R1. [CrossRef]
42. Shapiro, C.R.; Gayme, D.F.; Meneveau, C. Generation and decay of counter-rotating vortices downstream of yawed wind turbines in the atmospheric boundary layer. *J. Fluid Mech.* **2020**, *903*, R2. [CrossRef]
43. Kleusberg, E.; Schlatter, P.; Henningson, D.S. Parametric dependencies of the yawed wind-turbine wake development. *Wind. Energy* **2020**, *23*, 1367–1380. [CrossRef]

44. Bastankhah, M.; Shapiro, C.R.; Shamsoddin, S.; Gayme, D.F.; Meneveau, C. A vortex sheet based analytical model of the curled wake behind yawed wind turbines. *J. Fluid Mech.* **2022**, *933*, A2. [CrossRef]
45. Narasimhan, G.; Gayme, D.F.; Meneveau, C. Effects of wind veer on a yawed wind turbine wake in atmospheric boundary layer flow. *arXiv* **2022**, arXiv:2210.09525.
46. Abkar, M.; Porté-Agel, F. Influence of the Coriolis force on the structure and evolution of wind turbine wakes. *Phys. Rev. Fluids* **2016**, *1*, 063701. [CrossRef]
47. Jonkman, J.; Butterfield, S.; Musial, W.; Scott, G. *Definition of a 5-MW Reference Wind Turbine for Offshore System Development*; Technical report; National Renewable Energy Lab. (NREL): Golden, CO, USA, 2009.
48. Churchfield, M.; Lee, S. NWTC dEsign Codes-SOWFA. 2012. Available online: http://wind.nrel.gov/designcodes/simulators/SOWFA (accessed on 3 October 2022).
49. Open Foam: The Open Source CFD Toolbox. 2019. Available online: http://www.openfoam.com/ (accessed on 3 October 2022).
50. Jonkman, J. *NWTC Design Codes (FAST)*; NREL: Boulder, CO, USA, 2010; Volume 44.
51. Churchfield, M.J.; Lee, S.; Michalakes, J.; Moriarty, P.J. A numerical study of the effects of atmospheric and wake turbulence on wind turbine dynamics. *J. Turbul.* **2012**, *13*, N14. [CrossRef]
52. Churchfield, M.; Lee, S.; Moriarty, P.; Martinez, L.; Leonardi, S.; Vijayakumar, G.; Brasseur, J. A large-eddy simulation of wind-plant aerodynamics. In Proceedings of the 50th AIAA Aerospace Sciences Meeting Including the New Horizons Forum and Aerospace Exposition, Nashville, TN, USA, 9–12 January 2012; p. 537.
53. Jha, P.; Churchfield, M.; Moriarty, P.; Schmitz, S. Accuracy of state-of-the-art actuator-line modeling for wind turbine wakes. In Proceedings of the 51st AIAA Aerospace Sciences Meeting including the New Horizons Forum and Aerospace Exposition, Grapevine, TX, USA, 7–10 January 2013; p. 608.
54. Wagner, R.; Cañadillas, B.; Clifton, A.; Feeney, S.; Nygaard, N.; Poodt, M.; St Martin, C.; Tüxen, E.; Wagenaar, J. Rotor equivalent wind speed for power curve measurement–comparative exercise for IEA Wind Annex 32. *J. Phys. Conf. Ser.* **2014**, *524*, 012108. [CrossRef]
55. Bromm, M.; Vollmer, L.; Kühn, M. Numerical investigation of wind turbine wake development in directionally sheared inflow. *Wind. Energy* **2017**, *20*, 381–395. [CrossRef]
56. Lundquist, J.; Churchfield, M.; Lee, S.; Clifton, A. Quantifying error of lidar and sodar Doppler beam swinging measurements of wind turbine wakes using computational fluid dynamics. *Atmos. Meas. Tech.* **2015**, *8*, 907–920. [CrossRef]
57. Blondel, F.; Cathelain, M. An alternative form of the super-Gaussian wind turbine wake model. *Wind. Energy Sci.* **2020**, *5*, 1225–1236. [CrossRef]
58. Shu, Z.; Li, Q.; He, Y.; Chan, P.W. Investigation of marine wind veer characteristics using wind lidar measurements. *Atmosphere* **2020**, *11*, 1178. [CrossRef]